

Excited-State Proton Transfer Dynamics of a Super-Photoacid in Acetone-Water Mixtures

Niklas Sülzner,^[a] Bastian Geissler,^[b] Alexander Grandjean,^[c] Gregor Jung,^[c] and Patrick Nuernberger*^[b]

Super-photoacids, that is, photoacids with a negative pK_a value in the electronically excited state, can trigger an excited-state proton transfer (ESPT) to the solvent. For the neutral pyranine-derived super-photoacid studied here, even indications for ESPT in acetoneous solution are reported. The characteristics of ESPT in this environment, that is, which intermediates exist and what the impact of cosolvents is, remain unsettled though. In this work, we study ESPT in acetone-water mixtures by steady-state and time-resolved fluorescence spectroscopy. Various effects are observed: First, the addition of water supports the formation of a hydrogen-bonded ground-state complex comprising one water molecule and the photoacid, whose excitation triggers the formation of a hydrogen-bonded ion pair on a sub-ns time

scale. Second, water has an overall accelerating effect on the fluorescence dynamics of the involved emitting species, whose contributions are disentangled in a global analysis scheme, enabling the identification of emission from the free photoacid, a photoacid-water complex, a hydrogen-bonded ion pair, and the deprotonated photoacid. At least two water molecules are necessary for ESPT in the environment. Third, additional acidification thwarts an efficient ground-state complex formation of the photoacid and water. However, upon excitation, complexation may occur on a timescale faster than the photoacid's excited-state lifetime, so that emission from a nascent complex emerges.

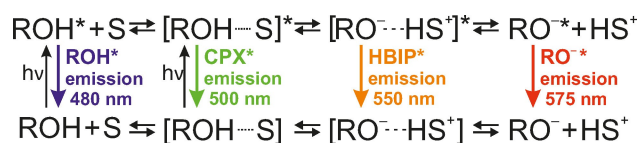
Introduction

Photoacids are molecules that exhibit an acidity increase upon irradiation, i.e., they are more acidic in an electronically excited state compared to the ground state.^[1] This behavior is typical for aromatic alcohols such as phenols,^[2–6] naphthols,^[7,8] or hydroxyquinolines.^[9] The prominent example, 8-hydroxypyrene-1,3,6-trisulfonate (pyranine, HPTS), is probably the most intensively studied photoacid of all.^[10–17] Triggered by photoexcitation, a photoacid can transfer its acidic proton more easily to suitable acceptors such as solvent or base, which makes an instance of an excited-state proton transfer (ESPT).^[18] Owing to the implementation of pulsed lasers, ultrafast time-resolved spectroscopy made it possible to monitor the ESPT process on its actual timescale.^[19,20] Moreover, the study of photoacids in different molecular environments allows for

elucidating mechanistic information on the ESPT process including the rate constants of the involved elementary reactions.^[21,22] However, only exceptionally strong photoacids with a negative pK_a value in the excited state, referred to as super-photoacids,^[23,24] are capable of performing ESPT in non-aqueous^[25,26] or aprotic solvents.^[27]

The Förster cycle represents the simplest thermodynamic description of photoacidity, only taking into account the excited-state and ground-state species of the protonated and deprotonated photoacid.^[28–30] More generally, the processes are described in a multi-step Eigen-Weller model^[31,32] (see Scheme 1) which includes that, besides the emission from the isolated photoacid ROH^* and the corresponding base RO^-* , further species can appear, namely a reaction complex (CPX) with a (co)solvent molecule S and a hydrogen-bonded ion pair (HBIP). Depending on the solvent's ability of separating ions, additional intermediates for the separation such as solvent-separated ion pairs (SSIPs) may also occur.

A few years ago, the Jung group introduced a promising, new class of pyranine-based photoacids that are substituted with strongly electron-withdrawing sulfonic ester groups.^[33]



Scheme 1. Eigen-Weller model for the ESPT processes of the photoacid studied in this work. The wavelengths indicate the spectral position of the fluorescence of the excited-state species.

[a] N. Sülzner
Lehrstuhl für Theoretische Chemie
Ruhr-Universität Bochum, 44780 Bochum (Germany)

[b] Dr. B. Geissler, Prof. Dr. P. Nuernberger
Institut für Physikalische und Theoretische Chemie
Universität Regensburg, 93040 Regensburg (Germany)
E-mail: patrick.nuernberger@ur.de

[c] A. Grandjean, Prof. Dr. G. Jung
Biophysikalische Chemie, Universität des Saarlandes
66123 Saarbrücken (Germany)

Supporting information for this article is available on the WWW under <https://doi.org/10.1002/cptc.202200041>

© 2022 The Authors. ChemPhotoChem published by Wiley-VCH GmbH. This is an open access article under the terms of the Creative Commons Attribution Non-Commercial NoDerivs License, which permits use and distribution in any medium, provided the original work is properly cited, the use is non-commercial and no modifications or adaptations are made.

These substituents do not only drastically enhance the photoacidity but they also provide an effective way towards non-charged super-photoacids. All photoacids of this class are characterized by large fluorescence quantum yields, high photostability, and high solubility in organic solvents. One of these photoacids, tris(1,1,1,3,3,3-hexafluoropropan-2-yl)-8-hydroxypyrene-1,3,6-trisulfonate (Scheme 2), is particularly strong with the pK_a dropping by more than eight orders of magnitude from 4.4 to -3.9 .

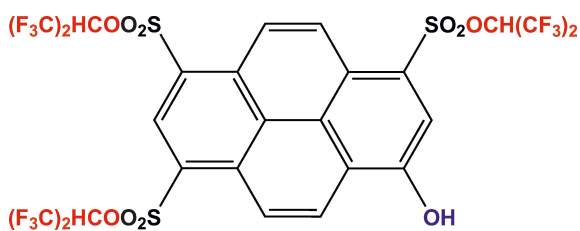
The solvatochromic effect of various solvents as well as the kinetic behavior in water, methanol, ethanol, and DMSO has been reported.^[34,35] Recently, the dynamics and intermediate species in a strongly hydrogen-bonded complex with a trialkylphosphine oxide was elucidated.^[36,37] Whereas most photoacids cannot transfer their proton to DMSO, the above-mentioned photoacid shows indications to do so even in the aprotic, weakly basic solvent acetone.^[34] However, for such a rather poor proton acceptor as acetone, traces of protic solvent admixtures like water can interfere in the ESPT process as a competing proton acceptor.

In this work, we present a systematic study on the effect of water on the excited-state proton transfer of this photoacid in acetone-water mixtures. Steady-state and time-resolved fluorescence spectroscopy on the picosecond to nanosecond timescale are used to unravel the excited-state dynamics. We show that four emitting species have to be considered to explain the emission dynamics, which are sensitive to the amounts of water admixtures and additional acid. Systematic variations of the solvent composition allow disentangling the individual contributions of the involved species.

Results and Discussion

The effect of water on the ground-state equilibrium

To investigate the possibility of water causing deprotonation of the photoacid already in the ground state, we studied the effect of water on the ground-state proton-transfer equilibrium prior to the time-resolved measurements. The steady-state absorption spectra shown in Figure 1(a) refer to samples with increasing amounts of water. A neutral solution of the photoacid typically exhibits two absorption features in accordance with previous findings: one maximum around 445 nm ascribed to the protonated form (ROH), and another one at 575 nm being characteristic for the deprotonated form (RO^-).



Scheme 2. Molecular structure of the investigated photoacid with highlighted sulfonic ester moieties (red) and hydroxyl group (blue).

Two observations can be made as the concentration of water, $[H_2O]$, increases:

First, spectral shifts occur with changing solvent composition. The ROH peak reveals a redshift while the RO^- peak undergoes a blueshift. Since in the acetone-water mixtures the polarity changes, this might be related to solvatochromism. The more water is present, the higher the polarity of the acetone-water solvent mixture^[38] and hence the better stabilized are the more polar states. Depending on the relative polarity of the electronic ground and excited state, this can either increase or decrease the $S_0 - S_1$ energy gap, leading to bathochromic or hypsochromic shifts, respectively. Despite the existence of several polarity scales, even for solvent mixtures,^[39] application of the Kamlet-Taft parameters appears especially appropriate to assign spectral shifts to specific solvent-solute interactions.^[13,34] Our observations for the acetone-water mixtures are in accordance with the previous results on solvatochromic effects for ROH and RO^- in polar solvents.^[34]

Second, the ROH peak intensity slightly increases under H_2O addition and, vice versa, the RO^- peak intensity decreases. Since water-induced deprotonation would cause more RO^- , the RO^- peak intensity decrease corroborates that ground-state deprotonation is negligible. Rather, the decrease can be rationalized by the formation of a photoacid-water complex in the ground state with slightly different spectroscopic properties (*vide infra*). Water-induced deprotonation starts to markedly affect the ground-state equilibrium only at water concentrations beyond 2 M (see Figure S1(a) in the Supporting Information).

Despite this rather high value before ground-state deprotonation sets in, we designed a new sample series using an initial amount of 6.5 mM of trifluoroacetic acid (TFA) to shift the ground-state protonation equilibrium to the protonated side. The steady-state absorption spectra in Figure 1(b) provide evidence that 6.5 mM of TFA is sufficient to shift the equilibrium completely to the protonated side due to the vanishing RO^- absorption band at 575 nm. Moreover, the equilibrium seems unaffected by water under acidic conditions as the RO^- signal does not reoccur with increasing $[H_2O]$ up to 1.09 M. The ROH absorption band reveals the same redshift as described before in combination with a weak decrease in absorbance. While there was only one reasonably defined isosbestic point for the spectra in neutral acetone (Figure 1(a)), there is an additional, yet still subtle one near 450 nm, i.e., in the ROH regime for acidic acetone. We note that solvatochromic shifts might be slightly different in the acidic environment compared to the neutral one, which could contribute to the observation of such an isosbestic feature. However, since also this one is substantially different from an isosbestic point corresponding to deprotonation (Figure S2), we assign the peak intensity changes of ROH also to the formation of a ground-state complex, in analogy to RO^- .

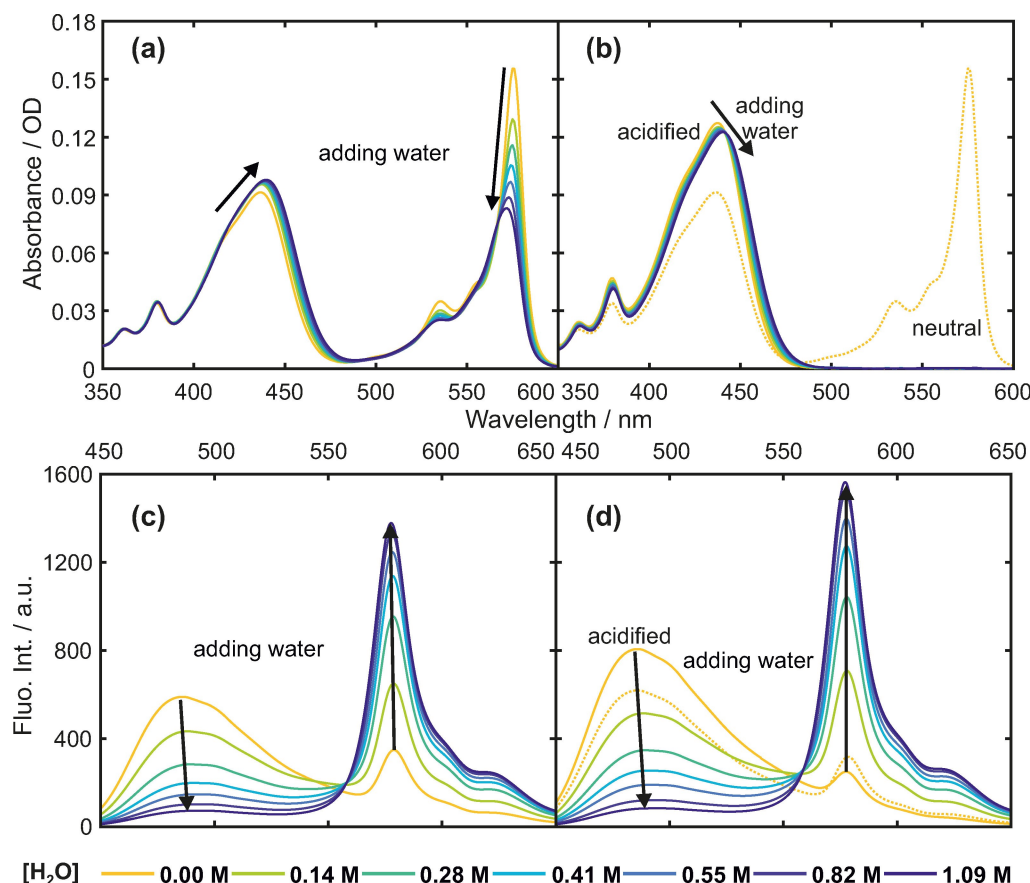


Figure 1. Steady-state characterization via UV/Vis absorption (top) and fluorescence emission (bottom) spectroscopy of samples with increasing concentration of water in neutral (left) and acidic (right) acetone solution. Fluorescence spectra (c, d) relate to 400 nm excitation. All samples refer to 20 μM photoacid while acidic solutions additionally contain 6.5 mM of TFA [with absorption spectra (a, b) being compensated accordingly to exclude dilution effects]. Concentrations of water are color-coded according to the legend. Arrows indicate the peak progressions upon the addition of water. The dotted lines in (b, d) refer to those neutral solutions in neat acetone without any additional water or acid from (a, c) as a reference.

Ground-state complex formation

Adduct formation between hydroxyaromatic compounds and hydrogen-bond acceptors, including common solvent molecules, is widely known for both the excited state and the ground state.^[40–43] With respect to ESPT in aprotic solvents, such hydrogen-bonded complexes (CPXs) between photoacids and additional bases have shown to affect the ESPT dynamics crucially because of the beneficial pre-coordination of the proton-accepting base. In fact, the CPX can represent the actual proton-transferring species of the photo-protolytic reaction cascade in aprotic environments, comprising two to three steps, as demonstrated for similarly strong photoacids in nitrile solution.^[36,37,44,45] Transferred to our system and in view of the spectral changes discussed above, this implies that a photoacid-water complex $\text{ROH} \cdots (\text{H}_2\text{O})_n$ could be formed in acetone as well if water is present. We suppose that such a complex provides a path for modified ESPT dynamics compared to the free photoacid. Based on the observed changes in the absorption spectra (Figure 1) as a function of the water concentration, we determined n , the number of involved water molecules, via Benesi-Hildebrand analysis^[46] represented by

Eq. (1) (derivation given in the Supporting Information). According to

$$[\text{H}_2\text{O}]^{-n} = Kd\Delta\epsilon[\text{ROH}]_0(\Delta A)^{-1} - K, \quad (1)$$

plotting $[\text{H}_2\text{O}]^{-n}$ against $(\Delta A)^{-1}$, where $\Delta A = A([\text{H}_2\text{O}]) - A(0)$ is the absorbance change at a given wavelength, should give a straight line. The intercept determines the association constant K of the complex, while the slope allows computing the difference attenuation coefficient $\Delta\epsilon$ as a function of K , path length d , and initial ROH concentration $[\text{ROH}]_0$. The exponent n is obtained by finding the best linear behavior. Figure 2 illustrates the Benesi-Hildebrand plots referring to absorbance changes at 450 nm, characteristic of ROH, under neutral and acidic conditions, as well as for the changes of RO^- at 580 nm. As can be seen, excellent agreement with the experimental data was found for $n = 1$. Based on that, we assume that neutral and acidic acetone solutions both contain the photoacid-water complex $\text{ROH} \cdots \text{OH}_2$ if water is present. In neutral solution (Figure 2(a)), the value of $(2.15 \pm 0.06) \text{ M}^{-1}$ for K suggests that already 23% of the photoacid is complexed after the first addition of water (0.14 M), while this fraction rises to 70% for 1.09 M of water. In contrast to this, the association

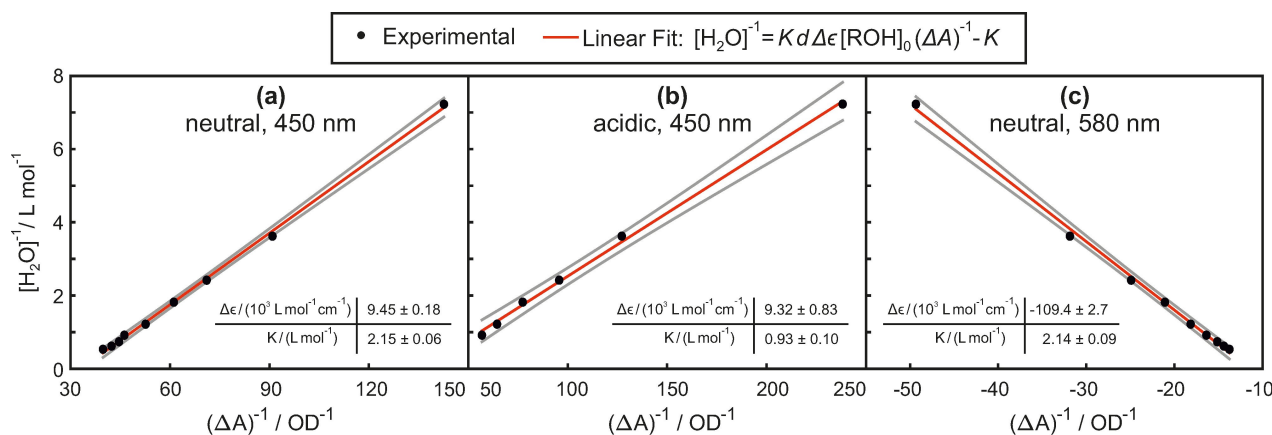


Figure 2. Benesi-Hildebrand plots ($[\text{H}_2\text{O}]^{-n}$ vs. ΔA^{-1}) based on the dilution-corrected absorption spectra for the neutral (a) and acidic (b) water series (cf. Figure 1) monitored at 450 nm, and monitored at 580 nm (c) for the neutral water series. Best linear fits were obtained for $n = 1$ (shown in red), with the 99% confidence intervals shown by gray lines. The fit results (slope and intercept) are included in the tables as insets.

constant is much smaller in acidic solution [$(0.93 \pm 0.10) \text{ M}^{-1}$] predicting lower complex fractions of 12% to 47% for water concentrations of 0.14 M to 1.09 M, respectively. Despite differing K values, the complexes can be considered equal because $\Delta \epsilon$ was found to be about $9400 \text{ L mol}^{-1} \text{ cm}^{-1}$ (for $d = 0.2 \text{ cm}$) under neutral ($[\text{ROH}]_0 = 16 \mu\text{M}$) as well as acidic ($[\text{ROH}]_0 = 20 \mu\text{M}$) conditions. Presumably, the complex $\text{ROH} \cdots \text{OH}_2$ is less stable in an acidic environment because of complex cleavage upon acidification. Since it is reported that water forms clusters in acetone^[47,48] and that the structure of water clusters changes upon protonation,^[49] we conjecture that water molecules prefer to be in the vicinity of a TFA molecule, which is a stronger acid than the ground-state photoacid.

For the absorption changes of RO^- , the best fit was also found for $n = 1$ (Figure 2(c)), with an association constant that is similar to the one for ROH in neutral solution. However, the magnitude of $\Delta \epsilon$ is much larger ($-109.4 \times 10^3 \text{ L mol}^{-1} \text{ cm}^{-1}$) which directly reflects the higher attenuation coefficient of RO^- compared to the one of ROH. In view of this, the aforementioned spectral shifts in Figure 1a and 1b comprise contributions from both solvatochromism and CPX formation.

The impact of water on the steady-state fluorescence spectra

Figure 1c and 1d depict the steady-state fluorescence emission spectra upon 400 nm excitation of the neutral (c) and acidic (d) sample series. Each spectrum consists of two characteristic emission signals with maxima around 480 nm and 575 nm, originating from the excited protonated species (ROH^*) and the excited deprotonated species (RO^{-*}), respectively. A direct comparison of 1c and 1d reveals no distinct differences between neutral and acidic conditions. Overall, the ROH^* emission intensity is generally slightly higher in acidic solution at all values of $[\text{H}_2\text{O}]$ due to a higher concentration of initially excited ROH^* by starting from a fully protonated system, as verified by the absorption spectra. For both sample series, the ROH^* emission signal strongly diminishes with increasing $[\text{H}_2\text{O}]$,

whereas the RO^{-*} signal rises. Only at concentrations larger than 2 M, the progression reverses and RO^{-*} intensity slightly decreases again (see Figure S1b). Moreover, the fluorescence spectra reveal an isoemissive point near 560 nm at both conditions, except for the spectra at 0 M water which behave differently.

We do not expect RO^{-*} emission after direct excitation of RO^- with 400 nm due to the small absorption cross section^[33] and the low concentrations of RO^- under acidic conditions. Even though the weak RO^{-*} signal could be still due to some initially excited RO^- , the observed water-dependence suggests that RO^{-*} must be additionally produced by some other photochemical process. Taking both progressions of ROH^* and RO^{-*} together, an excited-state proton transfer (ESPT) can be confirmed. Triggered by electronic excitation, ROH^* becomes more acidic than ROH and can thus transfer the acidic proton more easily, generating RO^{-*} .

A closer look at the ROH^* region also reveals that this emission signal is accompanied by a shoulder around 500 nm, causing a spectral broadening as a function of $[\text{H}_2\text{O}]$. Referring back to the complex formation in the ground state (*vide supra*), we assign this 500 nm feature to the excited photoacid-water complex CPX^* . As $[\text{H}_2\text{O}]$ increases, the solution contains increasing initial concentrations of CPX^* that start to dominate the ROH^* emission region. Considering hydrogen bonding as the likely bonding interaction in the complex, such a redshift of the fluorescence emission of the excited complex CPX^* relative to free ROH^* is also anticipated and experimentally observed for other systems. However, no isoemissive point between 480 nm (ROH^*) and 500 nm (CPX^*) is present, which fits to the changing initial ROH^* and CPX^* populations as a function of $[\text{H}_2\text{O}]$. By contrast, the observed isoemissive point near 560 nm refers to a subsequent reaction step with an additional proton-transfer intermediate in the excited state, which we assign to a hydrogen-bonded ion pair (HBIP). Such hydrogen-bonded species typically lie spectrally in between the excited protonated and deprotonated forms.^[50–52] To elucidate this, time-resolved fluorescence measurements were performed.

The effect of water on the fluorescence dynamics

Time-resolved fluorescence maps were recorded for the samples of Figure 1, i.e., for 14 values of $[\text{H}_2\text{O}]$ under neutral and 7 values under acidic conditions, four of which are illustrated in Figure 3 (see SI for further fluorescence maps, Figure S4). The maps in Figure 3 exhibit two major spectral features in accordance with the steady-state spectra. The first is an emission signal centered at 480 nm that occurs directly after excitation at $t=0$ ns ("time zero") and decays with a lifetime of about 4 ns at 0 M of H_2O . Concomitantly, another emission signal around 575 nm rises within about the same time constant (~ 4 ns) and decays with a longer lifetime (~ 6 ns). Both emission signals hence are kinetically correlated. When comparing the fluorescence maps for samples with increasing $[\text{H}_2\text{O}]$, it becomes apparent that water drastically alters the fluorescence kinetics. This can be followed by considering the kinetic traces taken at 480 nm and 575 nm, near the maximum positions, as shown in Figures 3(e) and 3(f). Thereby, the use of a logarithmic intensity scale allows testing for non-exponential decays since purely mono-exponential decays appear as straight lines in this representation.

On the one hand, the 480 nm signal referring to ROH^* emission yields a straight line for the water-free sample, corresponding to a monoexponential decay. Having water initially added, the ROH^* emission starts deviating from a monoexponential decay, which is reflected in a line curvature

of the plots as indicated by the curved arrow in Figure 3(e). This effect becomes the more severe the more water is present. Evidently, a faster decay of ROH^* that causes the more negative slope in the early time regime seems to superpose a slower decay represented by the less negative slope in the late time regime. Thus, the traces at 480 nm indicate a fluorescence decay becoming faster the more water is present.

On the other hand, the rise component of the 575 nm traces becomes steeper (in accordance with the corresponding shortened 480 nm decay), while the decay component remains almost unaffected, as demonstrated by the parallel lines in the late time regime of Figure 3(f). The combination of both eventually causes the intensity maximum at 575 nm to shift towards time zero, as indicated by the arrow.

The change caused by the first addition of water (0 M \rightarrow 0.14 M) behaves differently, as the 575 nm signal, referring to RO^-* emission, is very weak in water-free solution and hence constitutes a superposition of the actual RO^-* emission and the red tail of the ROH^* decay, which is maximal at 480 nm but not zero at 575 nm. The possibility of two further processes in the water-free sample, namely the ESPT to acetone and the interference with a trifluoroacetate anion, will be discussed below.

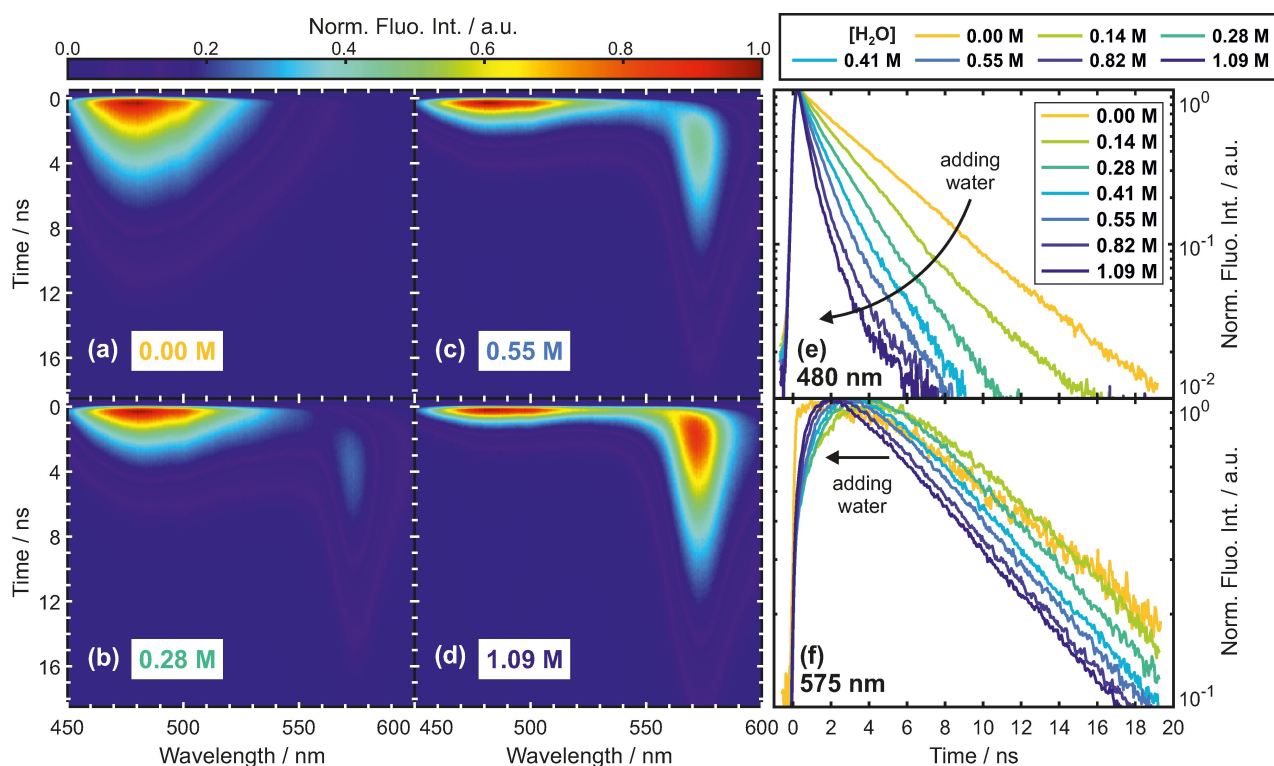


Figure 3. Normalized time-resolved fluorescence maps using 405 nm excitation for samples with increasing concentration of water (exemplarily (a) 0.00 M, (b) 0.28 M, (c) 0.55 M, (d) 1.09 M) in acidic solution (6.5 mM TFA) relating to Figure 1(d). All kinetic traces at 480 nm and 575 nm, taken from the maps, are compared on a logarithmic intensity scale in (e) and (f), respectively. Line colors refer to the concentrations as included in (e). Arrows indicate the progression when adding water.

The kinetic model for global analysis

All time-resolved fluorescence data was further analyzed in the context of the Eigen-Weller model of Scheme 1. A complete, numerical modeling^[53–55] with (diffusion-controlled) backreactions and equilibrations is very laborious and non-essential when the dynamic recombination is negligible, as indicated by the monoexponential decays in Figure 3(f).

In contrast to the trianion HPTS, the photoacid studied here is uncharged, so that diffusion contributions seem less relevant due to the weaker Coulomb attraction between the ions after ESPT. Moreover, Spies *et al.* demonstrated that the ESPT rates of this photoacid in H₂O, MeOH, and EtOH obtained from the exact, numerical solution to the Debye-Smoluchowski equation (DSE) are virtually identical to those determined by multi-exponential fitting.^[35] Besides, further studies on ESPT of similarly strong photoacids in other polar-aprotic solvents also presented kinetic analyses being in accordance with the experimental results, without explicitly solving the DSE.^[44,56–58]

Therefore, we apply a global analysis scheme^[59–62] with three parallel exponential decays in order to disentangle the emission processes. Details on the model are given in the SI.

Impact of water admixtures on the fluorescence dynamics

The results from the triexponential global analysis scheme for the water series in acidic solution are shown in Figure 4 (see corresponding residual maps in Figure S4 for assessing the fit quality), those in neutral solution are included in Figure S3 of the Supporting Information. Panels 4(a) to 4(c) display the decay-associated spectra (DAS), while the three rate constants are shown in Figure 4(d) as a function of the concentration of the water admixtures.

Similar to the steady-state fluorescence, the results for 0 M water differ from those with added water. We will thus first discuss those results after the first addition of water. At 0.14 M H₂O, the amplitude A_1 (Figure 4(a)) for the fastest component shows a large positive (decaying) contribution close to 475 nm, a negative (rising) contribution near 550 nm, and a small positive contribution at 575 nm. As [H₂O] increases, the 475 nm feature shifts to the red (reaching 480 nm) and gains in intensity while becoming significantly broader. At the final water concentration of 1.09 M, a shoulder near 500 nm becomes clearly visible. Meanwhile, the 550 nm contribution is also red-shifted, but its amplitude passes through a minimum of -0.5 and then slightly increases again with increasing water concentration. In parallel to this, the 575 nm feature loses in intensity. For an interpretation of the different contributions, we confer Scheme 1 and the different species therein. For illustrative purposes, as insets in Figure 4, the composition of the individual DAS is mimicked by spectral components representing these species. The component peaking at 480 nm is connected to the free (i.e., uncomplexed) photoacid, while the one at 500 nm refers to the excited photoacid-water complex CPX*. The negative signal at 550 nm corresponds to the rise of the proton-transfer intermediate HBIP*. The putative

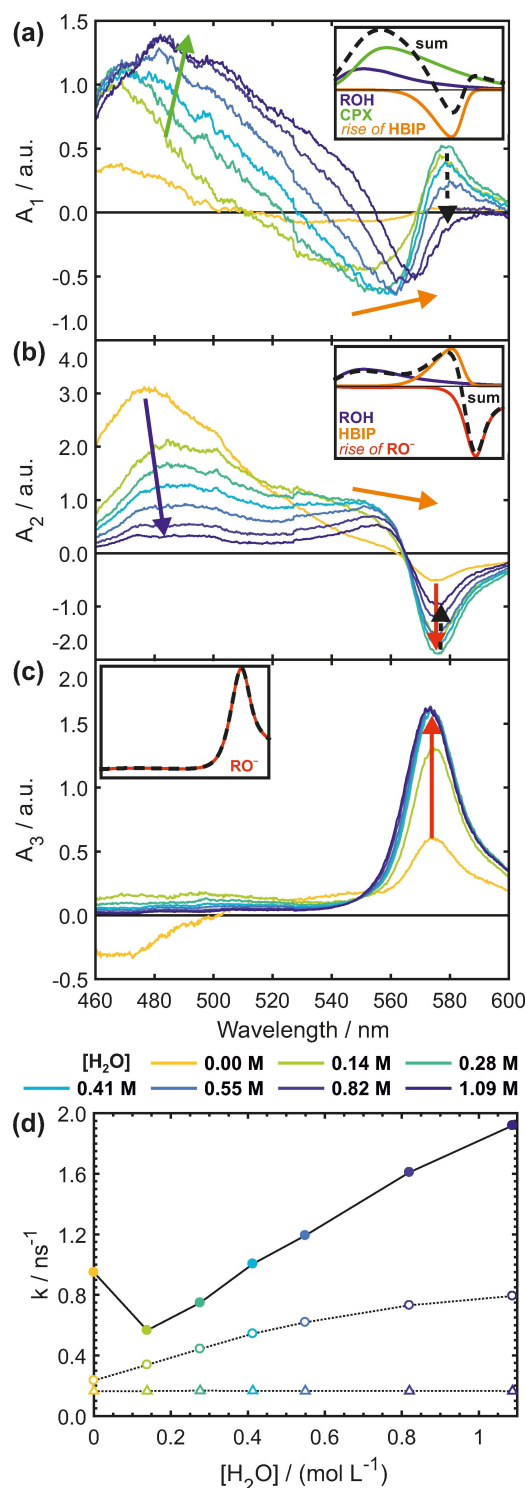


Figure 4. Results from a global analysis with three temporal components to the fluorescence intensity decay of the acidic sample series (Figure 3). Decay-associated spectra (DAS) relating to amplitudes A_1 (a), A_2 (b), and A_3 (c) are shown, together with a plot of the kinetic constants k_1 (filled circles), k_2 (open circles), and k_3 (open triangles), as a function of the concentration of water (d). The DAS comprise contributions from the four species ROH*, CPX*, HBIP*, and RO⁻ (Scheme 1). The insets of panels (a) to (c) provide a sketch to visualize the different contributions, which result in the overall DAS as indicated by the dashed black line. Note that the individual emission spectra change in shape and shift with an increase of the water concentration. This is indicated by the arrows whose colors correspond to the contribution given in the insets.

peak at 575 nm does not actually represent a decay contribution in the spectral region of the excited base, but is the result of a superposition of the ROH* (with decreasing contribution according to the steady-state complexation, see Figure 1), CPX*, and HBIP* (both with increasing contribution) spectra as indicated in the inset.

The corresponding rate k_1 (filled circles) shows an almost linear increase over the range from 0.14 M to 1.09 M with a slope of $\sim 1.5 \times 10^9 \text{ M}^{-1} \text{ s}^{-1}$, as suggestive for bimolecular reaction kinetics. However, since A_1 has contributions from both the ROH* and the CPX* decay in varying amounts, a direct assignment of the increase of k_1 to an acceleration of a distinct reaction step is intricate because of such kinetic mixing. Along these lines, the observed progression for k_1 basically reflects that HBIP* formation via CPX* is faster at higher water concentrations, and at least the magnitude of the apparent bimolecular rate constant strongly supports a diffusion-controlled reaction mechanism, which is the involvement of a further water molecule. Furthermore, no unambiguous indication for excited-state formation of RO^{-*} is found along with this fastest process in acidified solution, in contrast to neutral solution (see Figure S3). The participation of a further water molecule may be rationalized by the necessity of stabilizing a hydronium cation in acetone, which is facilitated if it is part of a hydrogen-bonded water cluster.

The second kinetic component A_2 (Figure 4(b)) is closely related to A_1 . Now, a strong positive contribution is observed, covering a broad range from 460 nm to 560 nm, that also shifts to the red during addition of water, but loses intensity in the spectral range of CPX*. Concomitantly, the amplitude peaks more and more around 560 nm, therefore adopting increasingly more CPX* and HBIP* decay character, in agreement with the complexation behavior. Furthermore, a negative contribution near 575 nm indicates that this component is coupled to the rise of RO^{-*}. Note that the overall spectra increase at 575 nm when water is added (black-dashed arrow in Figure 4(b)), but this is due to a superposition of the bathochromically shifting contribution of HBIP* (orange arrow in Figure 4(b)) and the increasingly negative feature of the RO^{-*} (red arrow). Therefore, we conclude that A_2 represents the time scale at which HBIP* turns into RO^{-*}, but also includes some contribution of emission from free ROH* on the short-wavelength side. A sketch of how the different species contribute is given in the inset of Figure 4(b).

The corresponding rate k_2 (open circles) increases with addition of water, initially in a linear fashion. This can be rationalized by the above-mentioned existence of water clusters in acetone, because for a HBIP to separate, the hydronium ion has to be stabilized, presumably via hydration in a water cluster, related to the long-standing debate of Zundel and Eigen complexes.^[63] Therefore, adding water facilitates the formation of RO^{-*} from HBIP*, but if there are enough water complexes present, the effect should cease to increase, giving rise to a maximum value of k_2 . Anyway, the observation that k_2 increases with a reaction order of $[\text{H}_2\text{O}]$ less than 1 suggests that higher oligomers ($n > 2$) are not mandatory for ESPT.

The amplitude A_3 of the slowest kinetic contribution only consists of a strong positive signal at 575 nm that is basically independent of the concentration of water. The corresponding rate constant k_3 (open triangles) does not change at all with water concentration. This can be understood given the assignment to the decay of RO^{-*}, a species which is not in contact with water cosolvent molecules and thus, may decay without a pronounced sensitivity on water concentration.

The instance of no water admixtures

The case of 0 M water behaves quite differently from the others. In the DASs, amplitude A_1 only has a comparably small 475 nm feature, but a rather broad negative contribution around 540 nm instead. The most pronounced DAS can be found for A_2 , which consists of a positive signal originating from ROH* and a negative signal representing the rise of RO^{-*}. We note that the characteristic feature at 550 nm observed with water admixtures and attributed to HBIP* is not present without water (see yellow curve in Figure 4(b)). Despite no additional water, we observe the RO^{-*} signal at 575 nm in A_3 . These three observations, (i) mainly ROH* in A_1 , (ii) no pronounced HBIP* in A_2 , and (iii) nonetheless RO^{-*} emission in A_3 , lead us to infer that an ESPT is also possible without water admixtures. Whereas the presence of water traces cannot be fully excluded and hence a signal contribution nonetheless involving water is conceivable, the remarkably different DASs imply that a distinct further mechanism is operative. Due to the high photoacidity of ROH*, it is conceivable that acetone actually acts as proton acceptor, as previously argued by Finkler *et al.*^[33] We note that the rate k_2 takes the value of 0.235 ns^{-1} , which is very close to the value of 0.234 ns^{-1} for the decay of the excited methoxy analogue ROME* which cannot transfer any proton (see Figure S5, ESI). Thus, if ESPT to acetone occurs, it has a much lower rate.

In addition, the slightly negative signal in A_1 together with the remaining positive signal in A_3 , both around 540 nm, further indicate that some of the ROH* molecules might form a complex which is not capable of ESPT and thus emits in this wavelength range. This behavior might originate in part from the involvement of trifluoroacetate anions, but also the occurrence of ESPT to acetone in the absence of water may play a role. Finally, the negative part of A_3 is not due to a real signal, but is probably a fit artefact that emanates from the similarity of k_2 and k_3 .

The impact of acid on the fluorescence spectra

As displayed in Figure 1, the addition of acid shifts the ground-state equilibrium towards ROH. Next, we aim to elicit whether there is a pronounced effect of acidification on the emission characteristics.

Starting with samples containing different amounts of water (for initial absorption spectra see Figure 1(b)), we added increasing amounts of TFA. Exemplarily, the steady-state

fluorescence spectra of three corresponding acidification series are illustrated in Figures 5(a–c). All spectra reveal the same progression with increasing [TFA] irrespective of the initial concentration of water, comprising a diminishing RO^{-*} emission (575 nm) coupled to an intensifying ROH^* emission (480 nm). Depending on the initial concentration of water, TFA achieves within the employed concentration ranges no complete, but only a partial restoring of the ROH^* emission intensity in water-free solution, as seen from the final spectrum of each series, i.e., those for highest [TFA]. It appears that the more water is present the more TFA is needed to restore the intensity referring to water-free solution.

Although a TFA excess suppresses the generation of RO^{-*} , the resulting spectra at high [TFA] do not fully resemble those in neutral or weakly acidic solution. Being most easily observable for the solution with highest $[\text{H}_2\text{O}]$ in Figure 5(c), a new emission signal at 550 nm emerges (red asterisk), becoming only apparent in highly acidic solution, in which the RO^{-*} emission is close to vanishing. From comparison with Figure 4, the 550 nm signal is identified as emission from HBIP^* . Thus, at high acid concentration, HBIP^* emission prevails instead of RO^{-*} .

We assume that this originates from a preference of water to be located in the vicinity of the stronger acid. Since this is the TFA if there is no excited molecule, the amount of water

being hydrogen-bonded to the photoacid is rather low. This has two implications. First, in case of an initial ground-state complex CPX , upon excitation CPX^* can form HBIP^* , but cannot further separate due to an insufficient number of water molecules to stabilize the separated ions. Second, in case of an initially isolated ROH , upon excitation ROH^* may encounter water molecules by diffusion, leading to a delayed rise of HBIP^* without further dissociation. To separate out the two contributions for HBIP^* formation, time-resolved fluorescence maps for all acidification series have been recorded.

The effect of acid on the fluorescence dynamics

Exemplarily, the corresponding kinetic traces at the emission maxima of ROH^* at 480 nm and of RO^{-*} at 575 nm are displayed in Figures 5(d–f). As the concentration of water increases, a pronounced deviation from the mono-exponential decay found above for a water-free solution is found for ROH^* , as is evident from the kink (black asterisk). Importantly, this kink disappears with increasing concentration of TFA, irrespective of the initial amount of water (as indicated by the curved black arrows). In contrast, the biphasic RO^{-*} signal is affected by TFA to a much lesser degree. Only the series for 0.14 M of water reveals a slight progression at 575 nm. For the others,

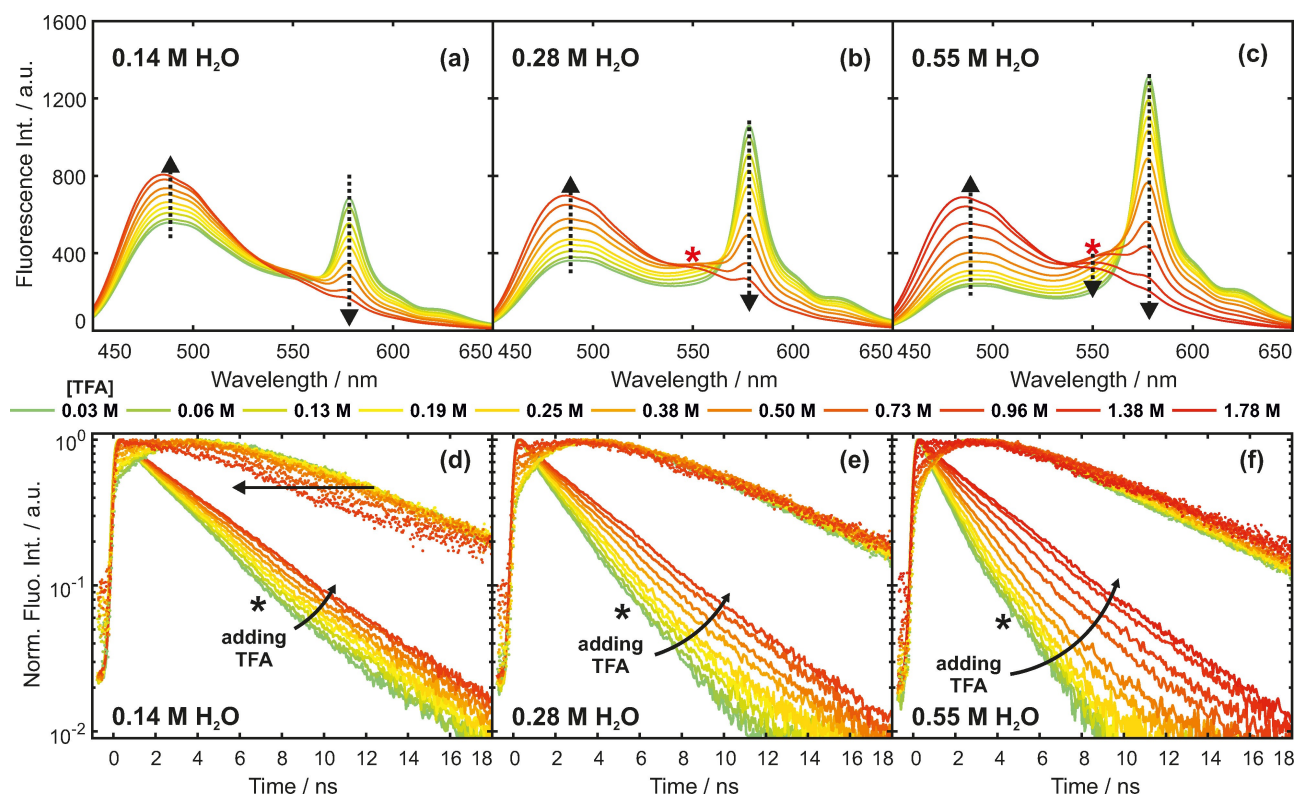


Figure 5. Emission from samples with increasing concentration of TFA after 400 nm (a–c) or 405 nm (d–f) excitation. Each column refers to a sample series with a specific concentration of water (0.14 M, 0.28 M, 0.55 M). Colors refer to the individual concentrations of TFA according to the legend. **Top row:** Steady-state fluorescence spectra. Black, dashed arrows indicate the peak progression with increasing TFA. Red asterisks highlight a new emission feature around 550 nm. **Bottom row:** Semi-logarithmic plots of selected kinetic traces at 480 nm (lower, solid lines) and 575 nm (upper, dotted lines) taken from the time-resolved maps of the samples with increasing concentration of TFA. Black asterisks indicate kinks in the profiles. Colors refer to the individual concentrations of TFA according to the legend. Solid arrows indicate the progression with increasing TFA.

merely the rise component vanishes, causing an overall shift of the maximum towards time zero, while the decay component remains mostly unaffected. These effects are mainly due to the spectral superposition of weak RO^{-*} emission (centered at

575 nm) to the red tail of the ROH* emission (extending to 575 nm).

In analogy to Figure 4, quantification of these effects on the fluorescence dynamics is accomplished by global analysis based on Eq. (S2) (SI), as displayed in Figure 6. The first row of

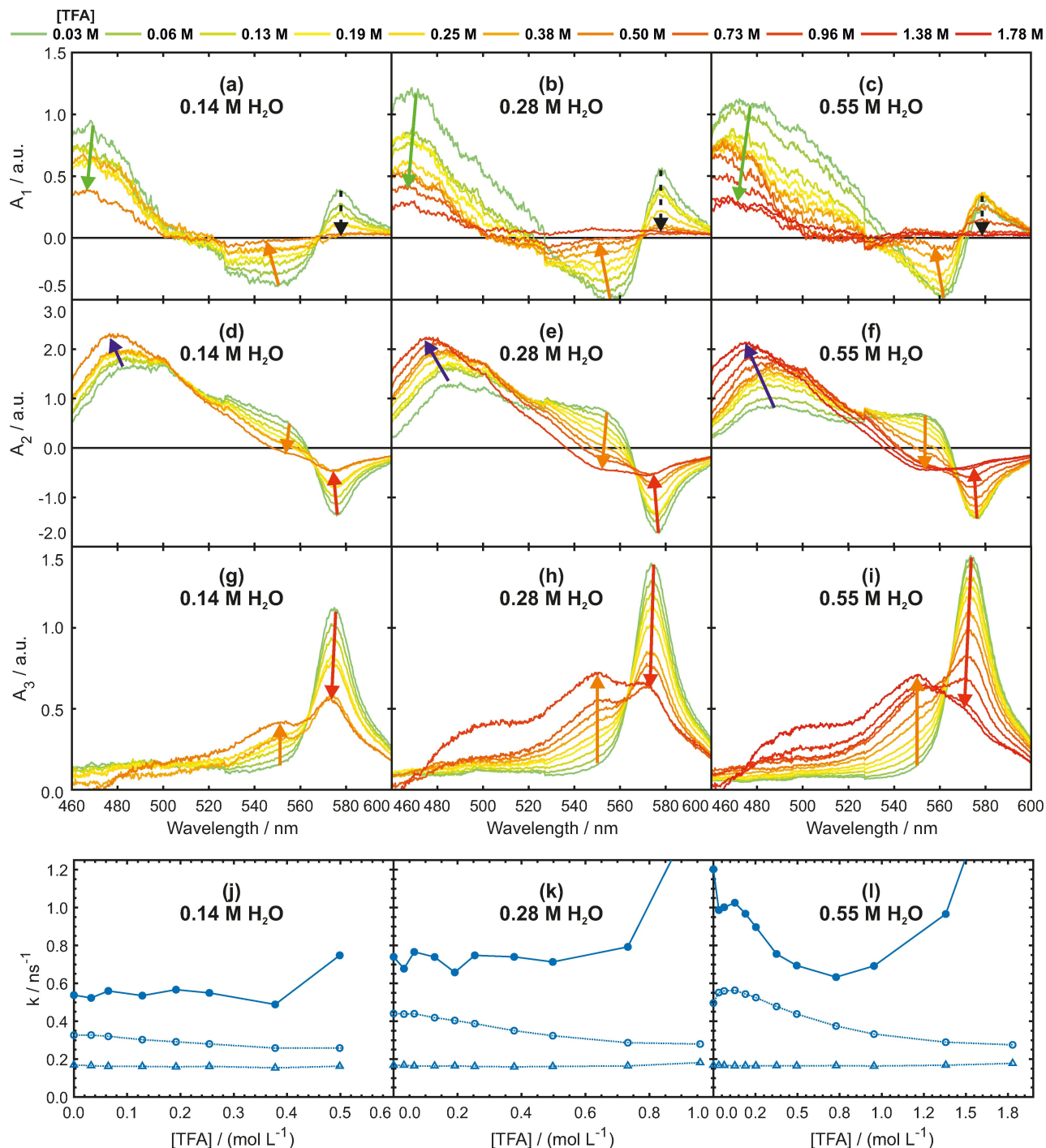


Figure 6. Results from a global analysis with three temporal components to the fluorescence intensity decay of the samples with increasing concentration of TFA (Figure 5). Each column refers to a sample series with a specific concentration of water (0.14 M, 0.28 M, 0.55 M). Colors refer to the individual concentrations of TFA according to the legend. Black, dashed arrows indicate the peak progression with increasing [TFA]. The peak progressions with increasing [TFA] are indicated by arrows whose colors refer to the contributing species, i.e., ROH* (blue), CPX* (green), HBIP* (orange), and RO^{-*} (red). **Upper three rows:** Decay-associated spectra (DAS) relating to amplitudes A_1 (a–c), A_2 (d–f), and A_3 (g–i). **Bottom row:** Plots (j–l) of the kinetic constants k_1 (filled circles), k_2 (open circles), and k_3 (open triangles) as a function of the concentration of TFA.

Figure 6 shows the effect of acidification on the DAS A_1 corresponding to the fastest dynamics. In the region below 520 nm and above 570 nm, the CPX* emission steadily decreases with increasing [TFA]. In the same manner, the negative signal observed in between, corresponding to HBIP* formation, decreases as well. This is in line with our interpretation that the water molecules gather around the strongest acid, i.e., around TFA rather than ROH, so that excitation yields the less CPX* the more TFA is present.

If this conclusion is appropriate, a decrease of CPX* should be accompanied by an increase of ROH* emission. This is indeed reflected in A_2 (Figure 6(d–f)) by the growth of the emission signal at 480 nm with increasing [TFA]. Moreover, the HBIP* emission around 550 nm in combination with the negative rise of RO[−]* at 575 nm should also shrink, as is evident in these DASs. It seems that the addition of TFA, at least at low concentrations, reverses the effect of water addition, see the comparison of Figure 6(a–f) and Figure 4(a–b).

Remarkably, for the highest value of [TFA], the DAS A_2 even becomes negative in the spectral region around 550 nm. Thus, this signal indicates a rise of HBIP* emission that does not originate from a previous CPX*. Rather, we propose that a water molecule encounters an excited photoacid ROH* in a diffusive process, directly yielding HBIP*. This can be rationalized as ROH* now is the stronger acid than TFA, in contrast to the situation in the ground state.

Further in line with our interpretation, the RO[−]* emission at 575 nm constantly diminishes with increasing [TFA], reflected in DAS A_3 in Figure 6(g–i). At high values of [TFA], A_3 starts to exhibit a positive contribution peaking at 550 nm and, for the highest TFA concentration, even a broad emission around 500 nm. This shows that HBIP* and even CPX* are formed more slowly and persist for a longer time compared to weakly acidic solution. Our explanation is again based on initial TFA-water complexes which encounter a ROH* molecule and can lead to HBIP* formation. Because this complex is already acidic, a full separation of HBIP* to yield RO[−]* does not occur and, in the extreme case of very high [TFA], even HBIP* formation is hindered, giving rise to the emission signal of CPX*, persisting on the longest observed timescale. The putative formation of a [ROH...TFA]* complex under these conditions might further contribute.

The discussed processes are also reflected in the rate constants (Figure 6(j–l)). Corresponding to the fastest dynamics, k_1 describes the conversion of CPX* into HBIP* (*vide supra*). Since acidification only reduces the amount of CPX*, A_1 shrinks but k_1 stays almost constant. The actual value of k_1 depends on the water concentration (also compare to Figure 4(d)). The reason for the decrease of k_1 in Figure 6(l) is again rationalized by the proposed clustering of water around TFA, effectively reducing the amount of water in the vicinity of the photoacid, so that a value of k_1 is approached which would correspond to less water in the non-acidic case. In other words, TFA inhibits the formation of HBIP*, which shows signatures of diffusion-controlled reaction kinetics (cf. Figure 4(d)). We conjecture that this analogously affects k_1 in Figure 6(j–k), but to a lower extent. In the extreme case of strongly acidic conditions, there

is basically no water close to the photoacid and hence, no CPX in the ground state. Consequently, there is also no initial CPX* after excitation and, in the global analysis, k_1 rather mimics the solvation dynamics of ROH*. This process occurs on ps time-scales so that the actual value of k_1 is meaningless because of limited time resolution. Since the solvation dynamics lead to a bathochromic shift with time, the amplitude A_1 for the initial emission of ROH* is therefore still slightly blue-shifted with respect to the steady-state emission of ROH* (compare the maximum at 470 nm in the curves for highest acid concentration in Figure 6(a–c) vs. 480 nm as found in Figure 1(c–d)).

With increasing acidification, the rate constant k_2 undergoes a change from describing the HBIP*→RO[−]* conversion to the diffusive HBIP* formation from ROH* with approaching water (see the sign change of the amplitude assigned to HBIP* in Figure 6). For large TFA excess, it appears that k_2 approaches the same value of about 0.27 ns^{−1}. We note that this is again close to the radiative decay rate of 0.234 ns^{−1} for the methylated analog ROME* (see Figure S5 in ESI), i.e., a situation where emission only originates from the initial species.

The rate constant k_3 takes the same value for all studied water concentrations (also see Figure 4(d)) and low [TFA], because it then solely represents the RO[−]* emission, as already evident from the corresponding DAS A_3 . Time-resolved studies using time-correlated single-photon counting (TCSPC) and fluorescence up-conversion report that RO[−]* emission decays monoexponentially with a rate constant of 0.18 ns^{−1} in DMSO,^[33] 0.17 ns^{−1} in water,^[35] and 0.17 ns^{−1} in MeOH and EtOH.^[35] We find a value of 0.17 ns^{−1}, in very good agreement with these other studies. At high [TFA], further contributions from HBIP* and CPX* mix in as described before, causing a slight increase of k_3 .

Summary

Our experiments have investigated the emission characteristics of a super-photoacid ROH in acetone-water environments. For the dynamics, we found that global analysis with a tri-exponential model allows a comprehensive interpretation of the data. Our five main findings are:

(1) ESPT even in neat acetone

The observation of RO[−]* emission without any water admixtures and the concomitant decay of ROH* with virtually the same rate as ROME* implies that ESPT to acetone might also be possible, yet very inefficient. In steady-state fluorescence studies, this possibility has already been suggested^[33] and is now supported by our time-resolved analysis.

(2) CPX formation in the ground state upon water addition

If water is used as a cosolvent, steady-state absorption and emission spectra reveal that a complex between the photoacid

and water is formed in the ground state. A Benesi-Hildebrand analysis disclosed that this complex CPX comprises one water molecule and the photoacid.

(3) A three-step Eigen-Weller model can explain the fluorescence dynamics in the presence of water

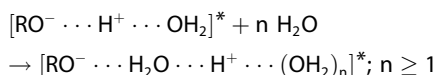
Excitation at 405 nm generates ROH* and, to an increasing degree with rising water concentration, CPX*. The latter subsequently transforms into HBIP*, which may further give rise to RO^{-*} (if there are sufficient water molecules, see finding (4)). Signatures of all four species involved in this three-step Eigen-Weller model can be clearly identified both in steady-state and time-resolved emission spectroscopy.

Excited contact ion pairs as the most prominent ESPT intermediates are commonly short-lived (few-ps) in water,^[56,64,65] though this is not necessarily the case in polar-aprotic solvents. For experiments with our photoacid and trioctylphosphine oxide in nitriles, CPX* and HBIP* intermediates have been shown to be necessary as well to describe the emission characteristics adequately.^[36,37] If ground-state dynamics are additionally monitored, as done by Vester *et al.*^[51] in photon antibunching experiments for this photoacid in DMSO, a further solvent-separated ion pair needs to be taken into account.

Recently, Kumpulainen *et al.* reported that ESPT to DMSO of a 1,8-naphthalimide-based photoacid ($pK_a^* \sim -2$), which is similarly strong to ours, proceeds according to a two-step Eigen-Weller model *via* a contact ion pair that is generated by a fast, solvent-controlled initial proton-transfer equilibrium.^[56] Further restraining proton dissociation by changing to even less polar solvents then gives rise to the need for complex formation with an additional base prior to the ESPT, overall requiring a description based on a three-step model.^[57] Albeit it is a different photoacid, the employed model has great similarities to the one used by us.

(4) More than one water molecule required for HBIP* separation

By analyzing the titration series with water, it became apparent that HBIP* cannot separate if no further water molecules are in close vicinity. We conclude that a hydrogen-bonded network is necessary to stabilize the hydronium cation:



This observation has some analogy to the reactivity of diphenylcarbene (DPC) in methanol/acetonitrile mixtures,^[66,67] in which, depending on the solvent composition, photo-generated singlet DPC can only abstract a proton from a methanol molecule if the generated methoxide anion is stabilized by hydrogen bonds to other methanol molecules.

(5) Acidification of acetone-water mixtures reduces the local hydration of the photoacid

TFA is a stronger acid than the ground-state photoacid. Thus, if TFA is added to an acetone-water mixture containing the photoacid, our data shows that the amount of water molecules adjacent to the photoacid declines, and in turn CPX*, HBIP*, and, finally, RO^{-*} is suppressed after excitation. It is known that water can form clusters in acetoneous environments,^[47,48] which we assume to be located around TFA rather than ROH.

Under high concentration of TFA, there is hardly any CPX present in solution since all the water gathers around TFA. Photoexcitation thus initially leads to almost exclusively ROH* emission. However, HBIP* subsequently starts to emerge, but without preceding CPX* emission. In our interpretation, the HBIP* can be directly formed from ROH* and water which first have to encounter each other in a diffusive process. This effect is supposed to become the more distinct the more TFA is present, because then less ground-state complexation of the photoacid and water occurs. At large excess of TFA, even CPX* is observed which also originates from this diffusive mechanism.

Outlook

The ESPT dynamics of the neutral super-photoacid employed here can vary significantly in acetone-water mixtures depending on the solvent composition and the acidification. This opens two perspectives. On the one hand, desired emission properties are attainable if the environmental conditions can be tuned in a controlled manner. On the other hand, recording the emission in a variable environment also allows to obtain information on the latter. These versatile properties could be further manipulated by employing solvent mixtures with perturbed hydrogen-bond dynamics,^[68–74] applying high pressures^[26,75–77] or spatially encapsulating the compound. The latter approach was demonstrated for other photoacids confined in small solvent droplets,^[16] as e.g. also possible in (reverse) micelles,^[24,78–86] or small container molecules,^[87–89] which further alters the ESPT characteristics.

Acknowledgements

We thank Prof. Martina Havenith (Ruhr-Universität Bochum) for providing streak camera equipment and Dr. Anne Leutzgen (formerly Saarland University) for providing the photoacid. Different aspects of this work were supported by the Deutsche Forschungsgemeinschaft (DFG, German Research Foundation) within the Research Training Group "Confinement-controlled Chemistry" (Grant GRK2376, Project 331085229), under Germany's Excellence Strategy – EXC 2033 – 390677874 – RESOLV, and through Grant JU 650/8-1. Open Access funding enabled and organized by Projekt DEAL.

Competing financial interests

The authors declare no competing financial interests.

Data Availability Statement

The data that support the findings of this study are available from the corresponding author upon reasonable request.

Keywords: Eigen-Weller model · excited-state proton transfer · photoacid · solvent effects · time-resolved spectroscopy

- [1] E. Pines, Chapter 7 in “The Chemistry of Phenols”, edited by Z. Rappoport; John Wiley & Sons, Ltd, **2003**, DOI: 10.1002/0470857277.ch7, part of *Patai's Chemistry of Functional Groups*.
- [2] G. Granucci, J. T. Hynes, P. Millié, T.-H. Tran-Thi, *J. Am. Chem. Soc.* **2000**, *122*, 12243–12253.
- [3] M. Lukeman, P. Wan, *J. Am. Chem. Soc.* **2002**, *124*, 9458–9464.
- [4] N. Basarić, P. Wan, *Photochem. Photobiol. Sci.* **2006**, *5*, 656–664.
- [5] M. K. Nayak, P. Wan, *Photochem. Photobiol. Sci.* **2008**, *7*, 1544–1554.
- [6] S. Kaneko, S. Yotoryama, H. Koda, S. Tobita, *J. Phys. Chem. A* **2009**, *113*, 3021–3028.
- [7] E. Pines, D. Tepper, B.-Z. Magnes, D. Pines, T. Barak, *Ber. Bunsenges. Phys. Chem.* **1998**, *102*, 504–510.
- [8] L. M. Tolbert, J. E. Haubrich, *J. Am. Chem. Soc.* **1990**, *112*, 8163–8165.
- [9] T. G. Kim, M. R. Topp, *J. Phys. Chem. A* **2004**, *108*, 10060–10065.
- [10] M. Rini, B.-Z. Magnes, E. Pines, E. T. J. Nibbering, *Science* **2003**, *301*, 349.
- [11] O. F. Mohammed, D. Pines, J. Dreyer, E. Pines, E. T. J. Nibbering, *Science* **2005**, *310*, 83–86.
- [12] E. T. J. Nibbering, H. Fidder, E. Pines, *Annu. Rev. Phys. Chem.* **2005**, *56*, 337–367.
- [13] G. Jung, S. Gerharz, A. Schmitt, *Phys. Chem. Chem. Phys.* **2009**, *11*, 1416–1426.
- [14] B. Cohen, C. Martin Álvarez, N. Alarcos Carmona, J. A. Organero, A. Douhal, *J. Phys. Chem. B* **2011**, *115*, 7637–7647.
- [15] N. A. Carmona, B. Cohen, J. A. Organero, A. Douhal, *J. Photochem. Photobiol. A* **2012**, *234*, 3–11.
- [16] N. Alarcos, B. Cohen, A. Douhal, *Phys. Chem. Chem. Phys.* **2016**, *18*, 2658–2671.
- [17] C. Hoberg, T. Ockelmann, J. Shee, P. Balzerowski, D. DasMahanta, F. Novelli, M. Head-Gordon, M. Havenith, *ChemRxiv*. **2022**, DOI 10.33774/chemrxiv-2021-60zjv-v2.
- [18] N. M. Trieff, B. R. Sundheim, *J. Phys. Chem.* **1965**, *69*, 2044–2059.
- [19] R. Simkovitch, E. Kisin-Finifer, S. Shomer, R. Gepshtein, D. Shabat, D. Huppert, *J. Photochem. Photobiol. A* **2013**, *254*, 45–53.
- [20] M. Premont-Schwarz, T. Barak, D. Pines, E. T. Nibbering, E. Pines, *J. Phys. Chem. B* **2013**, *117*, 4594–4603.
- [21] N. Agmon, *J. Phys. Chem. A* **2005**, *109*, 13–35.
- [22] R. Simkovitch, S. Shomer, R. Gepshtein, D. Huppert, *J. Phys. Chem. B* **2015**, *119*, 2253–2262.
- [23] K. M. Solntsev, D. Huppert, N. Agmon, *J. Phys. Chem. A* **1999**, *103*, 6984–6997.
- [24] L. M. Tolbert, K. M. Solntsev, *Acc. Chem. Res.* **2002**, *35*, 19–27.
- [25] T. Nakagawa, S. Kohtani, M. Itoh, *J. Am. Chem. Soc.* **1995**, *117*, 7952–7957.
- [26] N. Koifman, B. Cohen, D. Huppert, *J. Phys. Chem. A* **2002**, *106*, 4336–4344.
- [27] Y. Guo, X. Li, J. Zheng, G.-I. Zhang, J. Liu, W. Chen, *Optoelectron. Lett.* **2006**, *2*, 115–117.
- [28] T. Förster, *Naturwissenschaften* **1949**, *36*, 186–187.
- [29] T. Förster, *Z. Elektrochem. Angew. Phys. Chem.* **1950**, *54*, 42–46.
- [30] T. Förster, *Z. Elektrochem. Angew. Phys. Chem.* **1950**, *54*, 531–535.
- [31] M. Eigen, *Angew. Chem. Int. Ed.* **1964**, *3*, 1–19; *Angew. Chem.* **1963**, *75*, 489–508.
- [32] A. Weller, *Prog. React. Kinet.* **1961**, *1*, 187.
- [33] B. Finkler, C. Spies, M. Vester, F. Walte, K. Omlor, I. Riemann, M. Zimmer, F. Stracke, M. Gerhards, G. Jung, *Photochem. Photobiol. Sci.* **2014**, *13*, 548–562.
- [34] C. Spies, B. Finkler, N. Acar, G. Jung, *Phys. Chem. Chem. Phys.* **2013**, *15*, 19893–19905.
- [35] C. Spies, S. Shomer, B. Finkler, D. Pines, E. Pines, G. Jung, D. Huppert, *Phys. Chem. Chem. Phys.* **2014**, *16*, 9104–9114.
- [36] A. Grandjean, J. L. Pérez Lustres, S. Muth, D. Maus, G. Jung, *J. Phys. Chem. Lett.* **2021**, *12*, 1683–1689.
- [37] A. Grandjean, J. L. Pérez Lustres, G. Jung, *ChemPhotoChem* **2021**, *5*, 1094–1105.
- [38] J. Ortega, C. Rafols, E. Bosch, M. Roses, *J. Chem. Soc. Perkin Trans. 2* **1996**, 1497.
- [39] C. Reichardt, T. Welton, *Solvents and Solvent Effects in Organic Chemistry*, 4th ed., Wiley-VCH, Weinheim, **2011**.
- [40] H. Beens, K. H. Grellmann, M. Gurr, A. H. Weller, *Discuss. Faraday Soc.* **1965**, *39*, 183.
- [41] C. A. Hasselbacher, E. Waxman, L. T. Galati, P. B. Contino, J. B. A. Ross, W. R. Laws, *J. Phys. Chem.* **1991**, *95*, 2995–3005.
- [42] J. Juanos i Timoneda, J. T. Hynes, *J. Phys. Chem.* **1991**, *95*, 10431–10442.
- [43] P. B. Bisht, G. C. Joshi, H. B. Tripathi, *Chem. Phys. Lett.* **1995**, *237*, 356–360.
- [44] T. Kumpulainen, B. H. Bakker, M. Hilbers, A. M. Brouwer, *J. Phys. Chem. B* **2015**, *119*, 2515–2524.
- [45] Y. M. Lee, S.-Y. Park, H. Kim, T. G. Kim, O.-H. Kwon, *Methods Appl. Fluoresc.* **2016**, *4*, 024004.
- [46] R. L. Scott, *Recl. Trav. Chim. Pays-Bas* **1956**, *75*, 787–789.
- [47] A. Perera, F. Sokolić, *J. Chem. Phys.* **2004**, *121*, 11272–11282.
- [48] D. S. Venables, C. A. Schmuttenmaer, *J. Chem. Phys.* **2000**, *113*, 11222–11236.
- [49] T. S. Zwier, *Science* **2004**, *304*, 1119–1120.
- [50] R. Simkovitch, K. Akulov, S. Shomer, M. E. Roth, D. Shabat, T. Schwartz, D. Huppert, *J. Phys. Chem. A* **2014**, *118*, 4425–4443.
- [51] M. Vester, A. Grueter, B. Finkler, R. Becker, G. Jung, *Phys. Chem. Chem. Phys.* **2016**, *18*, 10281–10288.
- [52] M. Vester, T. Staut, J. Enderlein, G. Jung, *J. Phys. Chem. Lett.* **2015**, *6*, 1149–1154.
- [53] E. Pines, D. Huppert, N. Agmon, *J. Chem. Phys.* **1988**, *88*, 5620–5630.
- [54] N. Agmon, E. Pines, D. Huppert, *J. Chem. Phys.* **1988**, *88*, 5631–5638.
- [55] D. Huppert, S. Y. Goldberg, A. Masad, N. Agmon, *Phys. Rev. Lett.* **1992**, *68*, 3932–3935.
- [56] T. Kumpulainen, A. Rosspeintner, B. Dereka, E. Vauthey, *J. Phys. Chem. Lett.* **2017**, *8*, 4516–4521.
- [57] T. Kumpulainen, B. H. Bakker, A. M. Brouwer, *Phys. Chem. Chem. Phys.* **2015**, *17*, 20715–20724.
- [58] J. C. Penedo, M. Mosquera, F. Rodríguez-Prieto, *J. Phys. Chem. A* **2000**, *104*, 7429–7441.
- [59] R. Ihaka, R. Gentleman, *J. Comput. Graph. Stat.* **1996**, *5*, 299–314.
- [60] K. M. Mullen, I. H. van Stokkum, *J. Stat. Softw.* **2007**, *18*(3), 1–46.
- [61] J. J. Snellenburg, S. P. Liptonok, R. Seger, K. M. Mullen, I. H. M. van Stokkum, *J. Stat. Softw.* **2012**, *49*(3), 1–22.
- [62] S. P. Liptonok, P. Nuernberger, A. Lukacs, M. H. Vos, *Methods Mol. Biol.* **2014**, *1076*, 321–336.
- [63] D. Marx, M. E. Tuckerman, J. Hutter, M. Parrinello, *Nature* **1999**, *397*, 601–604.
- [64] O. F. Mohammed, D. Pines, E. T. J. Nibbering, E. Pines, *Angew. Chem. Int. Ed.* **2007**, *46*, 1458–1461; *Angew. Chem.* **2007**, *119*, 1480–1483.
- [65] A. Brenlla, M. Veiga Gutiérrez, M. C. Ríos Rodríguez, F. Rodríguez-Prieto, M. Mosquera, J. L. Pérez Lustres, *J. Phys. Chem. Lett.* **2014**, *5*, 989–994.
- [66] J. Knorr, P. Sokkar, S. Schott, P. Costa, W. Thiel, W. Sander, E. Sanchez-García, P. Nuernberger, *Nat. Commun.* **2016**, *7*, 12968.
- [67] J. Knorr, P. Sokkar, P. Costa, W. Sander, E. Sanchez-García, P. Nuernberger, *J. Org. Chem.* **2019**, *84*, 11450–11457.
- [68] P. Jacques, *Chem. Phys. Lett.* **1990**, *171*, 353–356.
- [69] S. Gupta, S. Rafiq, M. Kundu, P. Sen, *J. Phys. Chem. B* **2012**, *116*, 1345–1355.
- [70] S. Gupta, S. Rafiq, P. Sen, *J. Phys. Chem. B* **2015**, *119*, 3135–3141.
- [71] L. R. R. Santin, S. C. dos Santos, D. L. R. Novo, D. Bianchini, A. P. Gerola, G. Braga, W. Caetano, L. M. Moreira, E. L. Bastos, A. P. Romani, H. P. M. de Oliveira, *Dyes Pigment.* **2015**, *119*, 12–21.
- [72] D. Das Mahanta, D. Rana, A. Patra, B. Mukherjee, R. K. Mitra, *Chem. Phys. Lett.* **2018**, *700*, 50–56.
- [73] D. Das Mahanta, S. I. Islam, S. Choudhury, D. K. Das, R. K. Mitra, A. Barman, *J. Mol. Liq.* **2019**, *290*, 111194.
- [74] S. Wortmann, S. Schloeglmann, P. Nuernberger, *J. Org. Chem.* **2022**, *87*, 1745–1755.
- [75] M. Kondo, X. Li, M. Maroncelli, *J. Phys. Chem. B* **2013**, *117*, 12224–12233.

- [76] L. Grimmelmann, V. Schuabb, B. Tekin, R. Winter, P. Nuernberger, *Phys. Chem. Chem. Phys.* **2018**, *20*, 18169–18175.
- [77] J. Schroeder, D. Schwarzer, J. Troe, P. Vöhringer, *Chem. Phys. Lett.* **1994**, *218*, 43–50.
- [78] B. Cohen, D. Huppert, K. M. Solntsev, Y. Tsfadia, E. Nachliel, M. Gutman, *J. Am. Chem. Soc.* **2002**, *124*, 7539–7547.
- [79] S.-Y. Park, O.-H. Kwon, T. G. Kim, D.-J. Jang, *J. Phys. Chem. C* **2009**, *113*, 16110–16115.
- [80] K. J. Tielrooij, M. J. Cox, H. J. Bakker, *ChemPhysChem* **2009**, *10*, 245–251.
- [81] T. Mondal, A. K. Das, D. K. Sasmal, K. Bhattacharyya, *J. Phys. Chem. B* **2010**, *114*, 13136–13142.
- [82] M. D. Fayer, N. E. Levinger, *Annu. Rev. Anal. Chem.* **2010**, *3*, 89–107.
- [83] C. Lawler, M. D. Fayer, *J. Phys. Chem. B* **2015**, *119*, 6024–6034.
- [84] S. Panja, D. K. Khatua, P. Pramanik, M. Halder, *Chem. Phys.* **2018**, *510*, 1–9.
- [85] A. Das, S. I. Islam, D. K. Das, R. K. Mitra, *ACS Omega* **2018**, *3*, 5715–5724.
- [86] S. I. Islam, A. Das, R. K. Mitra, *J. Photochem. Photobiol. A* **2021**, *404*, 112928.
- [87] R. Gepshtein, P. Leiderman, D. Huppert, E. Project, E. Nachliel, M. Gutman, *J. Phys. Chem. B* **2006**, *110*, 26354–26364.
- [88] N. Basílio, C. A. T. Laia, F. Pina, *J. Phys. Chem. B* **2015**, *119*, 2749–2757.
- [89] A. S. I. Amer, A. M. M. Alazaly, A. A. Abdel-Shafi, *J. Photochem. Photobiol. A* **2019**, *369*, 202–211.

Manuscript received: February 11, 2022
Revised manuscript received: April 13, 2022
Accepted manuscript online: April 14, 2022
Version of record online: May 16, 2022